Marine Pollution Bulletin 65 (2012) 415–424

Contents lists available at SciVerse ScienceDirect

Marine Pollution Bulletin

journal homepage: www.elsevier.com/locate/marpolbul

Island shadow effects and the wave climate of the Western Tuamotu Archipelago (French Polynesia) inferred from altimetry and numerical model data

Serge Andréfouët [a,*], Fabrice Ardhuin [b], Pierre Queffeulou [b], Romain Le Gendre [a,1]

[a] IRD, UR 227 CoRéUs, BP A5, 98848 Nouméa cedex, New Caledonia
[b] Ifremer, Laboratoire d'Océanographie Spatiale, B.P. 70, 29280 Plouzané, France

ARTICLE INFO

Keywords:
Wave field
Island shadow effect
Altimeter
Wave model
Aquaculture
Society Archipelago

ABSTRACT

To implement a numerical model of atoll lagoon circulation, we characterized first the significant wave height (*Hs*) regime of the Western Tuamotu Archipelago and the local attenuation due to the protection offered by large atolls in the south Tuamotu. Altimetry satellite data and a WAVEWATCH III two-way nested wave model at 5 km resolution from 2000 to 2010 were used. Correlation between altimetry and model was high (0.88) over the period. According to the wave model, the archipelago inner seas experienced attenuated *Hs* year-long with a yearly average *Hs* around 1.3 m vs a minimum of 1.6 m elsewhere. The island shadow effect is especially significant in the austral winter. In contrast with southern atolls, Western Tuamotu experienced only few days per year of *Hs* larger than 2.5 m generated by very high *Hs* southern swell, transient western local storms, strong easterly winds, and during the passage of distant hurricanes.

1. Introduction

In coral reef environments, hydrodynamics is one of the major physical forcing factor controlling, among other key processes, trophic productivity, biodiversity accumulation, dominance of certain types of community structures and their vulnerability and resilience to disturbances (Madin and Connolly, 2006; Walker et al., 2008). Hydrodynamics can have two contrasted roles regarding recovery and resilience. For instance, on the one hand, it may contribute to recovery through current-driven larval dispersal. On the other hand, it may bring destruction of habitats by large waves and reef erosion (see Hopley, 2011, for updated encyclopedia entries and reviews on the subject). Reefs and lagoons are exposed differently to hydrodynamic forcing because of the natural variability at regional to local scales of tides, winds, waves and currents. Although the general action of hydrodynamics, and in particular waves, are well known, the proper quantitative characterization of the hydrodynamic regime of a specific site has been seldom achieved. This is true within a reef system, to understand the small scale variabilities present within an atoll, a bay or along a reef system (e.g. Kench 1998; Hoeke et al. 2011), but this is also true at archipelago-scale between islands and reefs.

Local variability in dominant communities, functioning and vulnerabilities at an archipelago scale are related to the modification, within the archipelago, of the meso-scale hydrodynamical patterns. For instance, the topology of islands and the induced sheltering between islands may substantially modify the local wind and wave and energy regime, and therefore modify the type of dominant communities (Goldberg and Kendrick, 2004). To date, three approaches have been conducted to characterize differences in wave exposure within an archipelago or around a large island. A qualitative approach where coastline stretches are ranked according to a relative level of protection ("sheltered", "exposed", etc.) (Goldberg and Kendrick, 2004), a quantitative approach where fetch-based model and GIS compute a time-integrated exposure (Ekebom et al., 2003) and a quantitative approach based on actual wave measurements, coupled with physical or biophysical models (Storlazzi et al., 2005; Hoeke et al., 2011).

In atolls, one of the main types of coral reef complexes in the world, three hydrodynamic domains can be defined: the oceanic forereef, the rim and the lagoon. The lagoon is a bounded body of water that is closed or open to exchanges with the ocean depending on the structure of the rim (Andréfouët et al., 2001). In atolls of the Tuamotu Archipelago (French Polynesia), lagoons are the prime locations for the development of pearl oyster aquaculture, tourism and reef fisheries (Andréfouët et al., 2006). The former is a dominant economic activity for the country (Andréfouët et al., 2012). The Western Tuamotu region is a geographic area of high economic importance. Three major atolls for the pearl oyster industry are present, namely Ahe, Takaroa and Manihi (Fig. 1). Historically, a

* Corresponding author. Tel.: +687 26 08 00; fax: +687 26 43 26.
E-mail address: serge.andrefouet@ird.fr (S. Andréfouët).
[1] Present address: Ifremer, LERN, Avenue du Général de Gaulle, 14520 Port-en-Bessin, France.

0025-326X/$ - see front matter © 2012 Elsevier Ltd. All rights reserved.
http://dx.doi.org/10.1016/j.marpolbul.2012.05.042

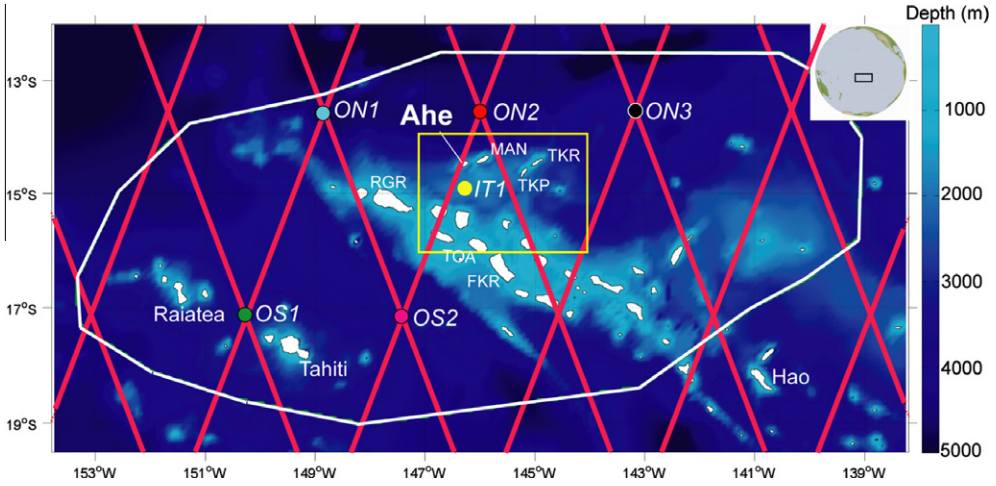

Fig. 1. Location map. In the centre of the Pacific Ocean, the Western Tuamotu (yellow box) and the focal atoll, Ahe, are shown, as well as the boundary of the WAVEWATCH III model (white line) at 0.05° resolution, the TOPEX-Jason acquisition tracks (red line), and the location of the six time-series of modeled *Hs*, five of them being in the ocean away from the atolls at the intersection of altimetry tracks (ON1, ON2, ON3, OS1, OS2) and one being a inner Tuamotu point (IT1), next to a track. Atolls and islands are in white. Atolls mentioned in the text: FKR: Fakarava, RGR: Rangiroa, TOA: Toau, MAN: Manihi, TKP: Takapoto, TKR: Takarao (For interpretation of the references to colour in this figure legend, the reader is referred to the web version of this article.).

fourth atoll of this area, Takapoto, was a major site in the eighties-nineties, but its black pearl industry collapsed and the focus shifted to the other atolls. Ahe was the target of a large interdisciplinary study between 2008 and 2010 (see collection of papers for this issue). Here, we focus the interpretation of our results on this atoll, although most of the conclusions remain valid for the other nearby atolls as well.

A wealth of empirical knowledge exists for each atoll and lagoon after more than 20 years of exploitation, but better knowledge on lagoon trophic and hydrodynamic functioning is a high priority for stakeholders in order to sustain a production of high quality pearls and understand how to optimize the collection of oyster larvae in the field (Thomas et al., 2012). Specifically, understanding the variability in spat collection is necessary. The success of this activity depends, in part, on how currents disperse larvae within the lagoon. Larvae dispersal can be studied by numerical solutions, and we followed this path to characterize the lagoonal circulation with the development of a 3D numerical model validated by field measurements (Dumas et al., 2012; Thomas et al., 2012).

Andréfouët et al. (2006) recommended first a proper characterisation of the atmospheric and oceanic forcing of the lagoon boundaries. In addition to tide, the wind and wave regimes were needed in priority. Indeed, it has been showed that wind directly influences the lagoon circulation, while ocean waves break along the rim and indirectly influence the lagoon by initiating water transport across the rim towards the lagoon (Atkinson et al., 1981; Tartinville et al., 1997; Kraines et al., 1999). Depending on the location, number and depth of spillways and passes along its rim, an atoll lagoon is efficiently renewed by a combination of tide and wave-driven flows through the rim (Kench, 1998; Tartinville et al., 2000; Andréfouët et al., 2001; Callaghan et al., 2006; Dumas et al., 2012).

During the first weeks of *in situ* work in Ahe in 2008, it appeared that the responses of flows through rim spillways to high swell events forecasted by Météo France meteorological services were unusually low, compared to our previous experiences in the Tuamotu (Andréfouët et al., 2001). In Andréfouët et al. (2001), we interpreted such peculiar low response to high swells by a specific rim geomorphology found in specific atolls (e.g. uplifted rims). This hypothesis cannot be ruled out, but these specific atolls were also protected by other atolls which effectively block the wave energy (e.g. Pawka et al., 1984). We hypothesized that the regional island shadowing effects due to the presence of other atolls could be responsible for the specific low responses of Ahe atoll to swell. The problem of the representation of atolls and islands in numerical models subgrids highlighted this shadow effect due to the atolls relative position, but the induced variation in swell amplitude within the archipelago remained undescribed (Chawla and Tolman, 2008; Delpey et al., 2010). Reasons for this poor knowledge are the absence of permanent *in situ* wave measurements, with only semi-quantitative wave information provided by atmospheric infrasound and seismic noise (Barruol et al., 2006). Therefore, an objective of the present study was also to quantify for the first time the significant wave height (*Hs*) attenuation around Ahe atoll due to the regional spatial distribution of atolls and islands. For this objective, we turned to quantitative satellite-based and modeling approaches.

In this study, we first provide a comparison of model *vs* altimetry data for the region of interest, at different spatial and temporal resolutions. As explained below, because altimetry data are relatively poor in spatial coverage and revisiting time, the model-altimetry data comparison is useful afterwards to justify the characterization of the wave regime using the model data only. Finally, using 11 years of modeled *Hs*, we identified the high wave events around Ahe atoll. The identification of these events using altimetry data alone would not have been possible given the short time these events may last, and, in some cases, their small spatial domain of influence.

2. Material and methods

2.1. Study site

The Western Tuamotu Archipelago is defined here by a box bounded by 14°–16° South- 144°–147° West, centered between the group of the main pearl oyster aquaculture atolls (Ahe, Manihi, Takapoto, Takaroa) and the barrier of the large south atolls (such as Rangiroa, Toau, Fakarava) (Fig. 1).

Local *Hs* measured in one location result from the propagation of wave fields across a larger region. The regional domain considered here is defined by a polygon including the Central Tuamotu, the entire Society Archipelago in the southwest corner, and about

2° of open Pacific Ocean north and south of the Tuamotu (Fig. 1). This configuration allows studying swell generated by distant storms when they reach the Western Tuamotu, as well as local wind-generated waves.

2.2. Characterisation of significant wave height and altimetry-model comparison

Here we investigate the spatial patterns of the wave field using a combination of satellite altimetry observation and numerical models. Satellite altimeter data has been shown to give very robust and accurate estimates of *Hs* (Queffeulou, 2004; Zieger et al., 2009; Queffeulou and Croizé-Fillon, 2010; Abdalla et al., 2011). The model is completely independent of the satellite data which is not assimilated. The model provides a daily full spatial and temporal coverage. This is an interesting complement to the satellite spatial and temporal coverage which is limited to narrow tracks (e.g. Fig. 1), revisited every few days at best (10 days for the TOPEX-Jason missions). The model also provides estimates of all sea state variables, and not just the *Hs* which is estimated by the altimeter. Thus, we also looked at the attenuation of waves for different dominant wave directions. For this we used the mean wave direction with a careful analysis of swell partition information. Indeed a mean direction in the presence of several wave systems can be completely meaningless.

The wave model is an implementation of a two-way nested WAVEWATCH III® modeling framework (Tolman, 2008, 2009, hereafter WW3). The two domains of interest are a 0.5° global grid in which a 0.05° resolution is nested. The extent of the inner domain is the white polygon shown in Fig. 1. It should be noted that the subgrid island blocking scheme of Tolman (2003, 2007) is used in both grids. These two domains are part of a set of grids used for forecasting and hindcasting (Magne et al., 2010). The wave model is forced by European Center for Medium-Range Weather Forecasts (ECMWF) operational analyses for the years 2006–2011 and by the Climate Forecast System Reanalysis (CFSR) (Saha et al., 2010) for the years 1988–2005. The sea ice mask is taken from CFSR or ECMWF, and for the years 2002–2009 it is complemented by a mask for small icebergs (Ardhuin et al., 2011a). Due to relative biases between these two wind fields, the model was re-tuned for CFSR winds by lowering the wind-wave growth term BETAMAX from 1.52 to 1.33. This provided a similar small bias in the two simulations and, in the model driven by CFSR winds, practically removed the important negative bias (−10% or so) for very large waves (*Hs* > 9 m) that was present in the model driven by ECMWF winds.

The two model domains use the wave generation and dissipation parameterizations proposed by Ardhuin et al. (2010). These parameterizations were specifically designed to match the swell dissipation that was measured over long distances with synthetic aperture radar data (Ardhuin et al. (2009a), Ardhuin et al. (2009b), Collard et al., 2009; Delpey et al., 2010). Finally, the model also includes coastal reflections for both resolved and subgrid shorelines, with a constant reflection coefficient of 5% and 10%, respectively, following a procedure described by Ardhuin et al. (2011b). WW3 output is given every 3 h. The hindcasted period runs from 2000 to 2010, for a total of 11 years. The full hindcast database is available at http://www.tinyurl.com/iowagaftp.

To complement previous global scale validations (Ardhuin et al., 2010), we re-examined altimeter observations in order to validate the WW3 model outputs in the western Tuamotu region. The altimeter significant wave height data are from the Ifremer altimeter *Hs* database (Queffeulou and Croizé-Fillon, 2010), which is updated regularly and calibrated using methods developed in Queffeulou (2004). Altimeter-derived *Hs* are provided along acquisition tracks with repeating visiting time that are different between missions and satellites (ERS-2, ENVISAT, TOPEX, Poseidon, Jason-1, Geosat Follow-On, Jason-2). A first comparison between WW3 and altimetry can be made for all concurrent data across the domain, during the entire period considered.

Then, to study *Hs* time-series around Ahe atoll for specific locations, and to maximize the number of collocations between altimetry and model during the 2000–2010 period, we used TOPEX and Jason acquisition tracks to identify five locations where altimetry and model could be optimally compared across time in our focal region (Fig. 1). These five locations correspond to the five open ocean track intersections which were the closest to Ahe atoll. The five points (ON1, ON2, ON3, OS1, OS2) were located at −13.5S, −148.75W; −13.5S, −146W; −13.5S, −143.25W; −17.25S, −150.25W; −17.25S, −147.50W, respectively. The revisiting time-period of TOPEX and Jason sensors provide one measurement every 10 days, yielding two measurements on a track intersection every 10 days. The 2002–2010 Jason-1 data set was expended with Geosat Follow-On (GFO) 2000–2008 data and with ENVISAT 2002–2010 data acquired near these points.

For all altimetry *vs* WW3 comparison, for any given day, the modeled *Hs* the closest in time with the altimetry *Hs* were used to compute monthly bias and standard deviations, thus the time difference was always lower than 1 h and 30 min.

2.3. Climatology of the Western Tuamotu wave regime

Since we aim to provide a first-order description of the swell regime in the Western Tuamotu based primarily on *Hs*, we did not use all the different wave variables provided by WW3. WW3 provides both wind wave and swell data and their different spectral decomposition, offering the possibility to discriminate different processes. Also full directional-frequency wave spectra have been stored at a few locations. In practice this information was not systematically used here since the total *Hs* and directions could often be readily interpreted in terms of trade-winds, events, and long-distance swell influence because of their preferential directions.

Monthly mean of WW3 *Hs* were computed to achieve a picture of the average situation, but to avoid a temporal smoothing effect of the spatial patterns, the 11 years of WW3 outputs for the regional domain were examined day by day to identify recurrent patterns of wave amplitude and directions, as well as events. Similar inspection of long term oceanographic spatial data were made by Soto et al. (2009) to detect short term dispersal of river plumes and transient river-coral reef connectivity using ocean color data from the SeaWiFS sensor. These wave events were short time periods of high *Hs* from any direction. Conversely, time periods of very low *Hs* were also interesting, since absence of waves have led to poor renewal of water in some atolls without passes, quick disequilibrium of the hydrological conditions, and dystrophic events (Adjeroud et al., 2001).

Altimetry data covers a longer time period than the WW3 period analyzed here. A monthly and 3-month mean, along-track, climatology of 1992–2010 *Hs* from the TOPEX and Jason missions was compiled. This *Hs* climate was obtained with TOPEX, Jason 1 and Jason 2 data covering respectively the period from 25/09/1992 to 11/08/2002; from 11/08/2002 to 26/01/2009; and from 26/01/2009 to 31/12/2010.

2.4. Quantification of the island shadow effect

Modelled *Hs* at the five locations ON1, ON2, ON3, OS1, OS2 were compared to modeled *Hs* at a sixth location (named IT1) in the south of Ahe atoll, in the centre of the Western Tuamotu box (Fig. 1). This inner Tuamotu location was used to measure *Hs* attenuation compared to open ocean *Hs* around the Western Tuamotu and in the region. In addition, the altimetry 1992–2010

climatology provided a mean to check with observations the long term influence of island on the Western Tuamotu wave regime.

3. Results and discussion

3.1. General patterns from altimetry and model-altimetry comparisons

The altimetry climatology (Fig. 2) shows that the Western Tuamotu, and especially the vicinity and the south of Ahe atoll, are areas of lower *Hs* compared to other regional values, all year-long. In December–February, northern swell modulates slightly this trend with *Hs* reaching 1.8 m next to Ahe, but from March to November, *Hs* remained below 1.6 m. Immediately south of the larger Tuamotu atolls, *Hs* was for the same period well above 1.8 m, thus a systematic decrease of at least 0.2 m between ocean and inner Tuamotu seas. Regionally, the north of the Tuamotu by 12°S and 142–146°W displayed between March and November a lower *Hs* compared to west of 150°W, where *Hs* was systematically above 2 m. The climatology thus suggests a significant island effect with lower *Hs* down-wave and down-wind from the atolls, especially with southern swell.

During the studied period, considering the entire data set (714,091 points, considering each available day and each altimetry sensor), the comparison of WW3 *vs* altimetry yielded a regression of $Hs_{WW3} = 0.834 \cdot Hs_{alt} + 0.152$, with a 0.88 correlation coefficient (Fig. 3). To test if the discrepancy could be explained by the time difference between the two *Hs* estimates, we kept only the data concurrent by <30 min. The overall correlation remained the same ($Hs_{WW3} = 0.838 \cdot Hs_{alt} + 0.144$, $n = 175{,}410$), but the correlation for large *Hs* (>4 m) was enhanced (not shown).

When looking at collocated time-series, *Hs* measured by the various altimetry missions and *Hs* from WW3 were in good agreement (Fig. 4), with a 5–15% underestimation by WW3. For the entire period, monthly standard deviations between the two data sets ranged between 0.2 and 0.3 m, except for few months. A significant increase in monthly bias occurred with ENVISAT in

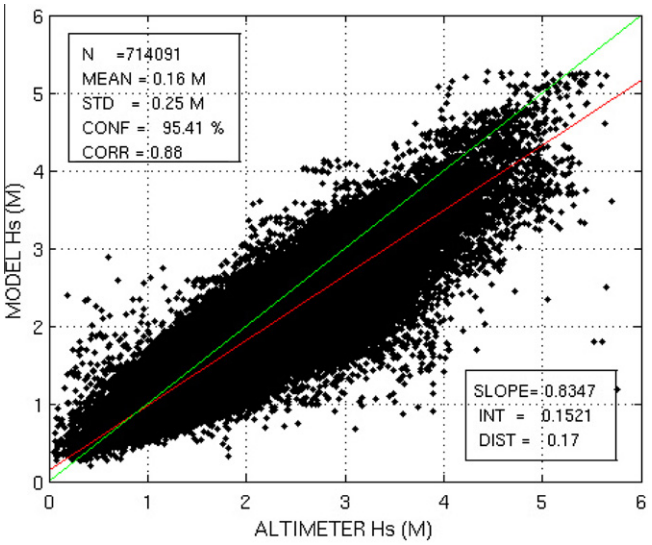

Fig. 3. Scatter-plot of collocated significant wave height (*Hs*) from altimetry and from the WAVEWATCH III model. Data were ±1 h 30 apart, corresponding to a spatial difference of 5–7 km at most. Data number (N), mean value (MEAN) and standard deviation (STD) of differences altimeter minus model *Hs*. Confidence level (CONF) and correlation (COR). Slope and intercept (INT) of the inertial regression line, average distance to the line (DIST). Red: inertial regression line. Green: $y = x$ line (For interpretation of the references to colour in this figure legend, the reader is referred to the web version of this article.).

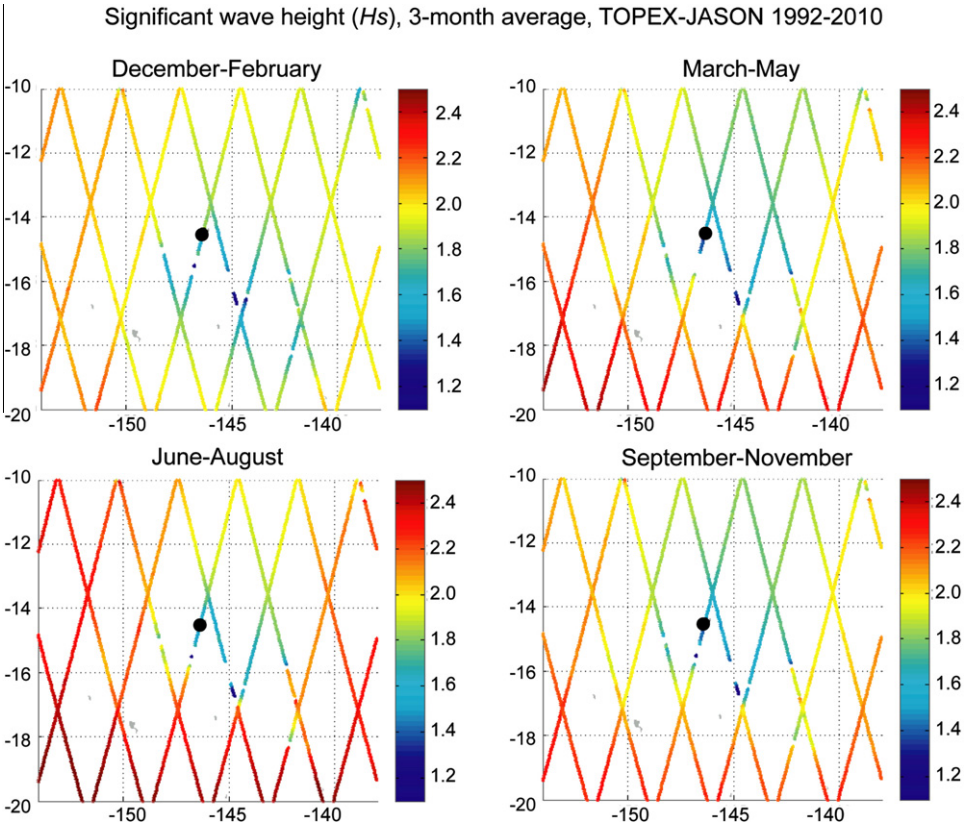

Fig. 2. Altimetry-derived 3-monthly mean *Hs* (in meters) plots for the period 1992–2010. The lowest *Hs* are observed in the south of Ahe atoll (black dot), in the north of the barrier made by the large atolls.

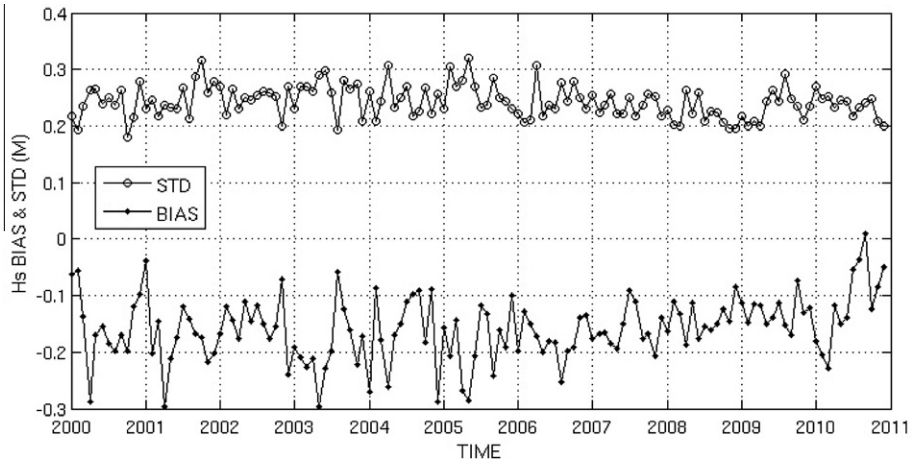

Fig. 4. Over the entire WAVEWATCH III high resolution spatial domain (Fig. 1), time-series of monthly bias and standard-deviation measured between the WAVEWATCH III significant wave height *Hs* and altimetric *Hs* estimated between 2000 and 2010 by Jason 1 (2002–2010), GFO (2000–2008) and ENVISAT (2002–2009).

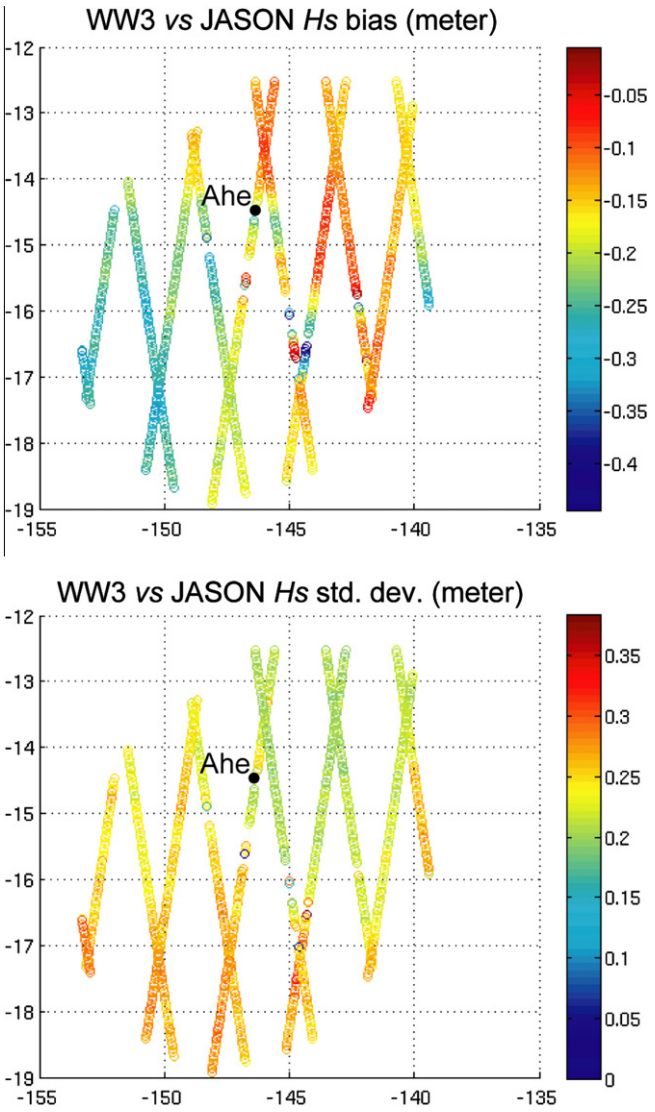

Fig. 5. Over the entire period of observations, spatial variations in the domain of interest (Fig. 1), along Jason altimetry tracks, of standard deviation and bias between WAVEWATCH III and altimetry-derived significant wave height (*Hs*, in meters) (For interpretation of the references to colour in this figure legend, the reader is referred to the web version of this article.).

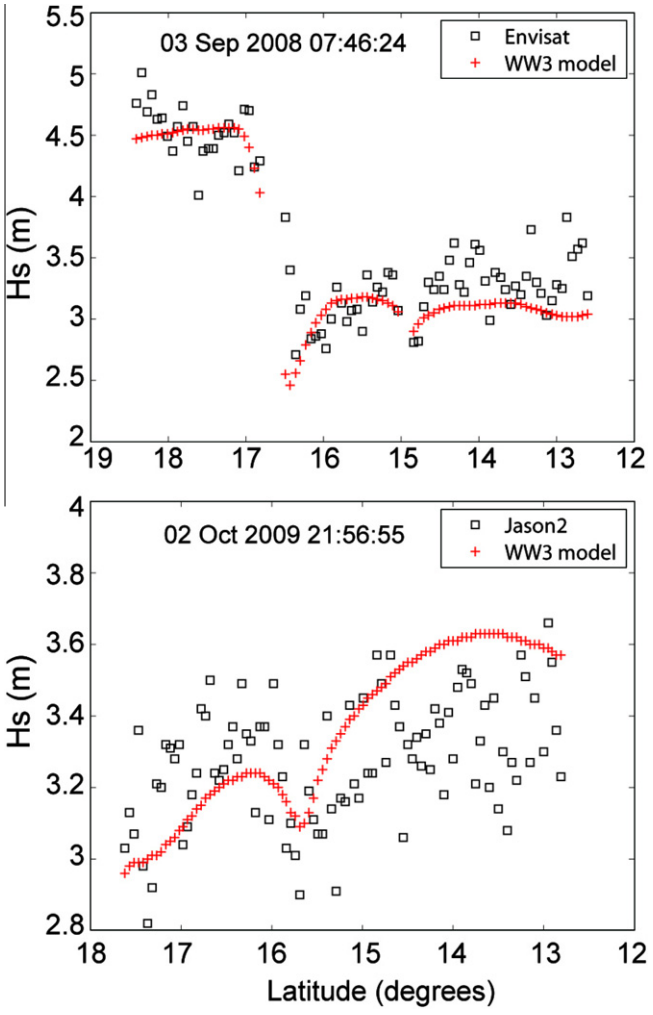

Fig. 6. For two selected days of high *Hs* in the regional domain (see also Fig. 10), along-track altimetry *vs* WAVEWATCH III comparison of significant wave eight (*Hs*). Date and starting time of acquisition are shown. Time period of altimeter acquisition is about 3 min for each plot.

2010, and this year was discarded (data not shown). The reason was a change in ENVISAT processing starting in February 2010 (Queffeulou, 2011).

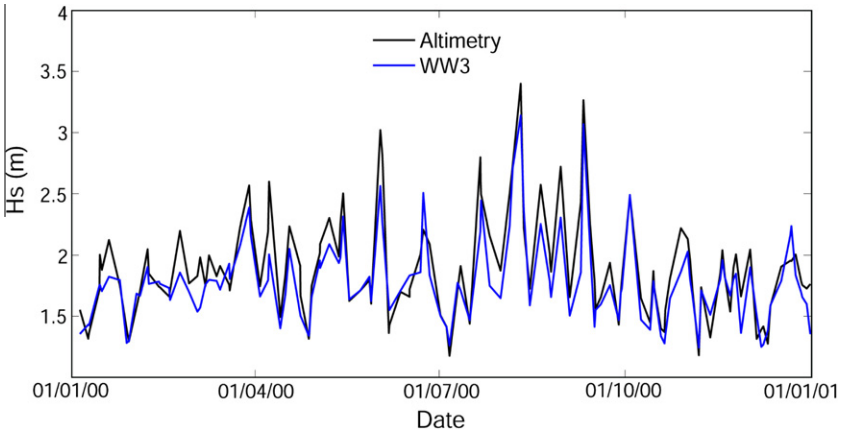

Fig. 7. Time-series of significant wave height (*Hs*) from WAVEWATCH III (WW3) and from altimetry for the year 2000, for one of the 6 focal points (ON1 here) shown Fig. 1. For each altimetry measurement, the most concurrent WW3 output is conserved.

The bias between altimetry and model varied spatially. When looking at the differences between WAVEWATCH III and the January 2002–January 2009 Jason data, overall, the pattern is a northeast to southwest increasing gradient (Fig. 5). Within this gradient, a patch of local higher discrepancy is evident in the south of Ahe (in green Fig. 5a), although the discrepancy is only about 5 cm higher than nearby values and is not as high as in the ocean domain of the southwest corner of the domain. These observed local discrepencies could reflect some difficulty in modeling accurately the shelter effect of small islands. The bias suggests a general underestimation of *Hs* by the model, compared to altimetry.

Looking at modeled *vs* altimetry data along an altimeter track for a particular day clarifies the dispersal of observations over a short time interval. As an example, for two specific days of high *Hs* in the domain, Fig. 6 shows the dispersal of the model *vs* altimetry data along one acquisition track, during a period of altimeter data acquisition lasting <3 min. The overall trends are in agreement, but with both underestimation and overestimation of *Hs*, around ±0.2–0.5 m for any specific moment in time.

Specifically for the 5 selected locations (ON1, ON2, ON3, OS1, OS2), the agreement between WW3 and altimetry was similar to that of the entire domain, with some interannual variations. An example of time-series for the year 2000 for ON1 is shown in Fig. 7. For the data in Fig. 7, the linear regression relationship was $Hs_{WW3} = 0.764 \cdot Hs_{alt} + 0.340$, $n = 132$.

In conclusion, for all the different time and spatial scales for which we compared WW3 and altimetry (Figs. 3–7), we found a good agreement, and more importantly a clarification of the range of uncertainties we needed to account for before concluding on *Hs* variations in the domain of interest. With this information in hand, WW3 high resolution results could be used with confidence to characterize the wave climate and assess the island shadow effects on *Hs*.

3.2. Island effects, wave regime and events

Besides the altimetry climatology observations that suggest an island effect in the Western Tuamotu (Fig. 2), time series of high resolution 0.05° WW3 *Hs* data at the 6 locations of interest confirmed that location IT1, in the south of Ahe and protected by other atolls, has a consistent significantly lower *Hs* year round, for all years, than all the other locations (Fig. 8). The yearly average at IT1 is systematically 0.3–0.35 m lower than at ON2, and 0.5–0.6 m lower than at OS2 (Fig. 8). Among the 5 other locations, considering the yearly average (Fig. 8), there is clear ranking that reveals the cumulated level of protection of each location. ON1, despite its northern location, is directly protected only in the case of south eastern wave. For south and south-western swells, ON1 is far less protected by Society Islands than ON2 and ON3 by the Tuamotu.

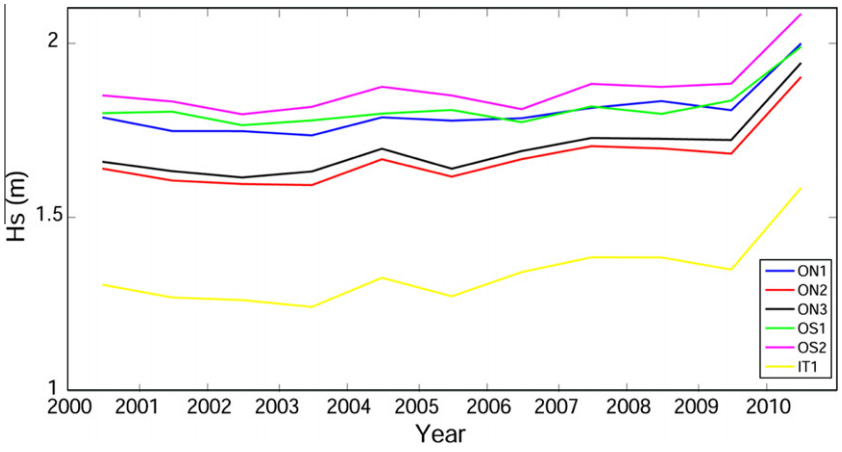

Fig. 8. Yearly average of WAVEWATCH III significant wave height (*Hs*) for the 6 locations (Fig. 1). IT1, the most protected location, is well separated from the 5 other oceanic ones. A group made of OS1, OS2 and ON1 have higher average *Hs* than the group made of ON2 and ON3. The ranking is consistent with the level of protection offered by the Tuamotu and Society Island since ON1 is not in the lee of the Tuamotu for southwest and south swells.

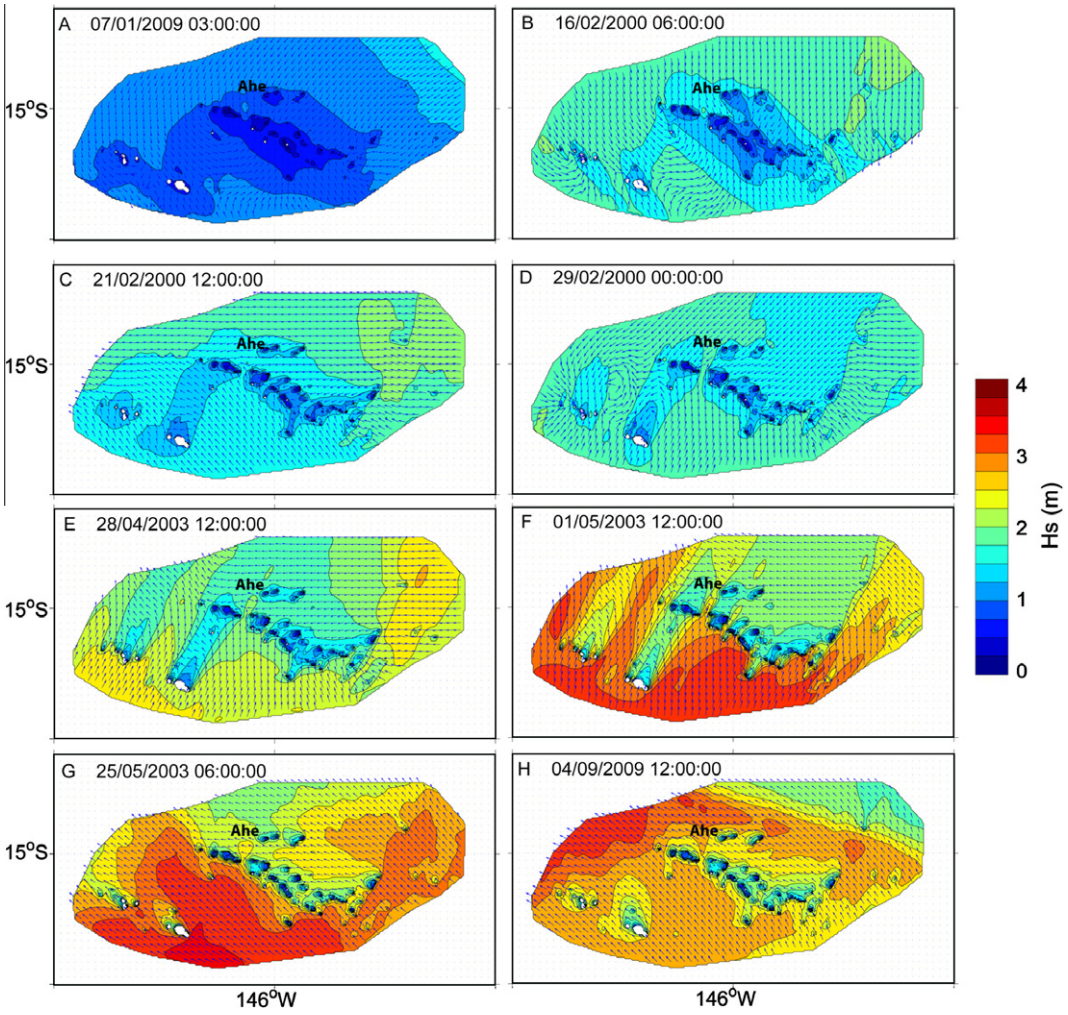

Fig. 9. Typical configurations of WAVEWATCH III significant wave height *Hs* in the region and in the Western Tuamotu. Selected days and hours are shown to highlight the intricate spatial patterns occurring in the archipelago, without smoothing when averaging over a long period.

Ahe atoll and the Western Tuamotu are not always protected from waves. Examination of the high resolution *Hs* and directions allowed identifying the typical configurations occurring year long, for the processed decade, for which Ahe is impacted by waves or protected by nearby atolls (Fig. 9).

In the Austral summer (November–March), the wave regime is dominated by an overall low *Hs*. In the north, south and west of the Tuamotu, wave directions may vary respectively north to east, southeast to southwest, and southeast to northeast (going clockwise). Fig. 9a–d illustrates a range of these configurations, which result from the relative contributions of moderate swell from distant north latitudes and local wind wave. The Tuamotu Archipelago acts as a barrier to northern swell (Fig. 9a), and Ahe is not protected in that case. Wave direction was the most erratic north of the Society archipelago (location OS1, data no show).

Starting in the austral winter, in April and till October, the combination of stronger tradewinds (northeast–southeast, clockwise) and stronger southern swells results in a more complex wave conditions (Fig. 9e–h). It also stabilizes the mean wave direction north and west of the Society Archipelago. Northern swell (as in Fig. 9b) disappears. Periods of low *Hs* and calm occur between periods of moderate to high swells (Fig. 9e–h). This is the period where the spatial patterns generated by island shadow effects are the most variables. In particular, the Fig. 9e–h presents several configurations of island shadowing effects with wave trains coming from the southwest, south and southeast directions. Wave from the southeast are effectively blocked by the barrier of southern atolls (Fig. 9g), given the incidence angle between the direction of atolls and the direction of the waves. Otherwise, south and southwest wave trains can propagate within the archipelago on narrow corridors (Fig. 9f). Under these conditions, the wavescape is the patchiest, with substantial variations of *Hs* over short distances. Note also the quasi-steady dominant wave direction (east), north of the Tuamotu, under the tradewind influence. In the panels Fig. 9e–f, this east direction is perpendicular to the dominant direction south of Tuamotu. Note also the significant shadowing effect induced by Tahiti and Moorea islands in southwest conditions (Fig. 9e and f). The last panel Fig. 9h shows a configuration occurring in austral winter after a period of high wind from the southeast, which builds high *Hs* in the western part of the domain due to a long regional fetch.

It should be pointed out that *Hs* remained consistently below 2.5 m in these typical situations, even when waves reach the atoll (south–southwest directions). We investigated with WW3 how the regional domain and the western Tuamotu experienced high waves during short term (1–8 days) events. Events bringing high amplitude waves in the region (arbitrarily set at $Hs > 3.75$ m) could be categorized in 4 groups.

- Type 1 event: the southern swells generated by distant storms in high south latitudes can bring high northward *Hs*. These events occurred every year, between April and November

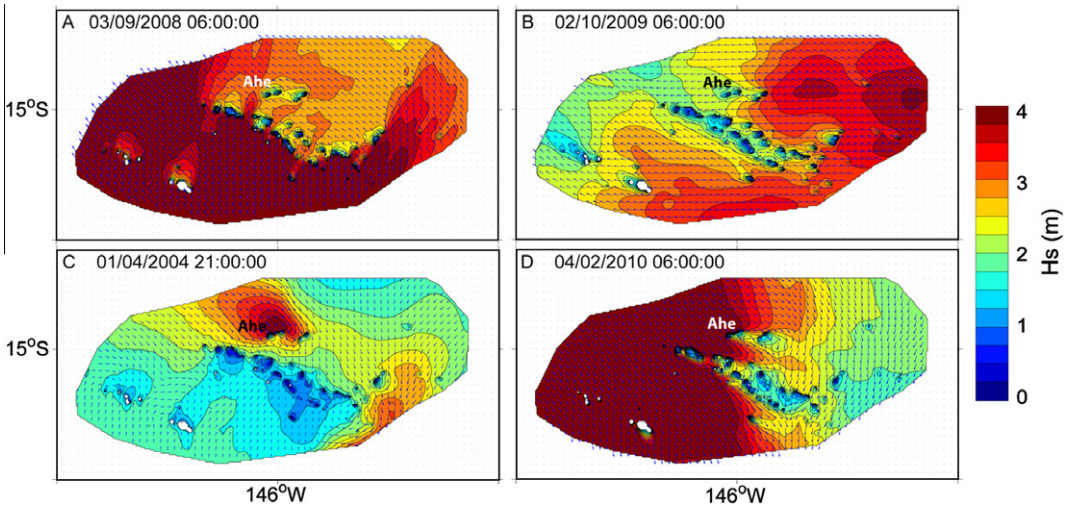

Fig. 10. Examples of remarkable events bringing significant wave height *Hs* above 3.75 m in the region, from the high resolution WAVEWATCH III model. Dates and hour are GMT time. Panels A–D represent respectively the event types 1–4 described in the text.

without clear repetitivity. They bring a region-wide increased *Hs*, up to 4.8 m in the south of the WW3 zoom area (Fig. 1) during 2–4 days. The most dramatic episode in the processed period occurred early September 2008 (Fig. 10a). Ahe appeared well protected during these events from the southern swell, but a cumulated effect of the residual southern swell and local wind waves brought *Hs* to 3.22 m (the yearly maximum, see Table 1), compared to 4.8 m next to Tahiti Island (at OS2). A tongue of northward wave crosses the Tuamotu, but Ahe itself is mostly impacted by wave generated by local eastern winds during these periods (Fig. 10a). Note also the significant shadowing effect induced by Tahiti-Moorea islands. Personal observations in Ahe in September 2008 confirm that no dramatic swells hit the atoll at this moment. Spillways reacted only moderately and the lagoon level did not reach an unusual value, continuing to oscillate according to tide variations (Dumas et al., 2012).

- Type 2 event: high waves with *Hs* > 3.75 m can be generated in the East of the regional domain by high easterlies wind, especially in June–September. Ahe is protected in this configuration by the two eastward atolls Takapoto and Takaroa. This type of event happened twice in 2009, corresponding to the strongest episodes recorded in the decade (Fig. 10b, Table 1).
- Type 3 event: Ahe atoll can be subjected to very localized waves generated by western transient storms (Fig. 10c). These are localized storms that cross in one or 2 days the regional domain. *Hs* reached up to 4 m on the northwestern side of Ahe during these events. These events did not occur every year, but Tuamotu experienced in 2004 and 2005 several of them (Table 1).
- Type 4 event: distant hurricanes generate high waves in the domain. The only example in our 11-year our time series was from hurricane Oli in early February 2010 (Fig. 10d). The hurricane passed in the southwest of the domain and seriously impacted the Australes Island in the south of French Polynesia. *Hs* reached 3.85 m around Ahe during this event, which is the highest *Hs* provided by the WW3 model in 11 years (Table 1).

The Figs. 9 and 10 are extracted from animations that show WW3 outputs across the 11 years of data. These animations are available on request to the authors.

No high *Hs* waves in our 11-year time series came from the North, from distant storms. Overall, Ahe atoll was subjected to *Hs* > 2.5 m only a few days per year (Fig. 7 and Table 1). In 2001, this threshold was reached for one day only (Table 1). Nevertheless, Ahe remains exposed to high waves generated by hurricanes and by western localized storms, although the later passed extremely quickly. It would be possible to further characterize more

Table 1
Summary of high WAVEWATCH III *Hs* for each year at location IT1 in the south of Ahe atoll (see Fig. 1). For instance, in 2010 during 26 days *Hs* was above 2.5 m. These 26 days consist in 5 periods of consecutive days throughout the year, one of them corresponding to an event of type 4, with the passage of hurricane Oli (lasting 8 days) that brought *Hs* up to 3.85 m that year. A day is included if *Hs* > 2.5 m for at least 3 h. An event is characterized by *Hs* > 3.75 m in the region (there are 4 different types of events, see text). An event occurring in the region may, or not, be related to the occurrence of the maximum *Hs* in IT 1. In 2007, 2006, 2002 and 2001, no concurrent events occurred in the region at the time of the maximum *Hs* but they were related to eastern waves, generated by local winds, so a process similar to the events of type 2.

Year	*Hs* max (m)	Date of *Hs* max	Related corresponding event	Total number of days with *Hs* > 2.5 m	Number of clusters of consecutive days with *Hs* > 2.5 m
2000	3.08	10-September	Type 1	4	2
2001	2.53	06-August		1	1
2002	2.59	01-October		2	1
2003	2.90	08-July	Type 2	7	3
2004	2.86	02-April	Type 3	3	2
2005	3.10	24-February	Type 3	4	2
2006	2.72	12-June		8	4
2007	2.78	30-August		8	2
2008	3.22	03-September	Type 1	8	3
2009	3.27	20-February	Type 2	17	6
2010	3.85	04-February	Type 4	26	5

finely these wave trains according to their periods, and quantify the level of vulnerability of Ahe for each different type of events. This will be part of a subsequent study.

3.3. WAVEWATCH III high resolution model and the characterization of coral reef exposure

To the best of our knowledge, this study is the first to use a 5 km high spatial resolution wave model to investigate the wave climate within a coral reef archipelago. The high temporal and spatial resolution allowed identifying trends and events, at a daily time-scale, and the spatial variability associated with the local topology of reef and islands. In comparison, to achieve at least one measurement per day, using only altimetry data would lead to enlarge substantially (up to 500 km) the spatial domain of integration around the focal study area (Tartinville and Rancher, 2000; Andréfouët et al., 2001).

Here, we only reported *Hs* results, and we used the decomposition between wind waves and swells provided by WAVEWATCH III to infer the source of the wave (local or distant) (not shown). This study is a first step of the analysis of the wave climate of a coral reef region before using more detailed outputs on all the available frequencies.

It could be possible to use other wave data sets spanning longer periods, such as the ERA-40 and ERA-Interim models. ERA Interim is the latest ECMWF global atmospheric reanalysis of meteorological observations from 1989 to the present, which displays major improvements over ERA-40 (1958–2001) (Dee and Uppala, 2009). However, their coarser resolution compared to the WAVEWATCH III model used here, and our direct use of altimetry data for a period long enough limit the interest of these models for our purposes. These data sets could be interesting to detect modifications of the wave regime due to climate change, but this is out of the scope of the present study.

The analysis performed here should be repeated elsewhere in other archipelagoes, possibly at higher spatial resolution thanks to availability of unstructured grids in most wave models (e.g. Benoit et al., 1996; Ardhuin et al., 2009a,b). Indeed, exposure to waves and wind is often a hydrodynamic parameter explaining the different type of communities existing on a section of reefs and the processes involved (see Edmunds et al., 2010 for a French Polynesia example, in Moorea Island). This exposure is seldom, if ever, quantified directly from observations or numerical wave models. Instead, other indirect GIS approaches based on wind climatology and fetch model have been used (e.g., Ekebom et al., 2003; Harborne et al., 2006; Burrows et al., 2008). The reason is that these methods, with little technical expertise, allowed answering the question of the influence of a time-integrated exposure on biological communities. But the development of online data servers providing high quality, high resolution wave model data similar to what we used here offers new perspectives for coastal ecologists (Hoeke et al., 2011).

3.4. Implications for Ahe atoll hydrodynamic functioning and modeling

In a companion study aimed at modeling the hydrodynamics of Ahe atoll lagoon (Dumas et al., 2012), *in situ* measurements of flows through the atoll rim in shallow spillways highlighted weak currents year round. Velocities and flows were responding to waves and tides fluctuations, but remained low compared to measurements made on other atolls (Andréfouët et al., 2001). This is a direct consequence of *Hs* attenuation around Ahe atoll, especially for southern swells. As a consequence, and considering the small number of functional spillways, flows generated by wave radiation stress were not a significant driver of the Ahe lagoon circulation, in contrast with other atolls like Majuro in Marshall Islands (Kraines et al., 1999). Thus, Dumas et al. (2012) parameterized the Ahe lagoon model with a standard, low, average flow at its boundaries, which allowed reproducing well a variety of physical and biological *in situ* measurements (Dumas et al., 2012; Thomas et al., 2012). This situation is likely specific, and besides the Takaroa, Manihi and Takapoto atolls located near Ahe, other less protected Tuamotu atolls would certainly need to use a realistic *Hs vs* velocity parameterization, especially for atolls with wide open reef flats such as Arutua, another important pearl oyster aquaculture site in the southern exposed part of the Tuamotu, which is directly facing the southern swells. Generalization from one atoll to another is certainly possible, but after quantification of the relative exposure of the different rim sections to swell energy.

4. Conclusion

This study (1) described the use of modeling tools to characterize the wave climate at high resolution in an archipelago environment, complementing previous use of scarce altimetry data and GIS fetch-model approaches; (2) it described the wave climate of one archipelago and highlights the temporal and spatial variations occurring at short distance due to the shadowing effects of islands relative to each others. Specifically, it shows that Ahe atoll, the focal atoll of a large interdisciplinary study, is subjected to an attenuated wave regime due to its northward sheltered position and is forced by an atypical wave regime compared to most other Tuamotu Archipelago atolls; (3) it justified the relaxed boundary rim-parametrization that has been implemented to model the atoll lagoon circulation (Dumas et al., 2012).

The combined use of high resolution wave model and altimetry data offers new perspectives to characterize the hydrodynamic forcing of numerous ecological, biological and geochemical processes in reef and lagoon environments. We predict that this study will pave the way for similar characterization elsewhere. In addition, this study has focused on the significant wave height regime only. Other aspects should be investigated in the future, including the energy of the wave trains according to their spectral decomposition.

Acknowledgements

This study was funded by the 9th European Development Fund (Grant POF/001/002N1 to S.A. and Loic Charpy, IRD) through the French Polynesia Service de la Perliculture. F.A. is supported by ERC Grant #240009 "IOWAGA" and US National Ocean Partnership Program, under Grant N00014-10-10383.

References

Abdalla, S., Janssen, P.A.E.M., Bidlot, J.R., 2011. Altimeter near real time wind and wave products: random error estimation. Marine Geodesy 34, 393–406.

Adjeroud, M., Andréfouët, S., Payri, C., 2001. Mass mortality of macrobenthic communities in the lagoon of Hikueru atoll (French Polynesia). Coral Reefs 19, 287–291.

Andréfouët, S., Pagès, J., Tartinville, B., 2001. Water renewal time for classification of atoll lagoons in the Tuamotu Archipelago (French Polynesia). Coral Reefs 20, 399–408.

Andréfouët, S., Ouillon, S., Brinkman, R., Falter, J., Douillet, P., Wolk, F., Smith, R., Garen, P., Martinez, E., Laurent, V., Lo, C., Remoissenet, G., Scourzic, B., Gilbert, A., Deleersnijder, E., Steinberg, C., Choukroun, S., Buestel, D., 2006. Review of solutions for 3D hydrodynamic modeling applied to aquaculture in South Pacific atoll lagoons. Marine Pollution Bulletin 52, 1138–1155.

Andréfouët, S., Charpy, L., Lo-Yat, A., Lo, C., 2012. Recent research for pearl oyster aquaculture management in French Polynesia. Marine Pollution Bulletin. 65, 407–414.

Ardhuin, F., Chapron, B., Collard, F., 2009a. Observation of swell dissipation across oceans. Geophysical Research Letters 36, L06607.

Ardhuin, F., Marié, L., Rascle, N., Forget, P., Roland, A., 2009b. Observation and estimation of Lagrangian, Stokes and Eulerian currents induced by wind and waves at the sea surface. Journal of Physical Oceanography 39, 2820–2838.

Ardhuin, F., Rogers, E., Babanin, A., Filipot, J.-F., Magne, R., Roland, A., van der Westhuysen, A., Queffeulou, P., Lefevre, J.-M., Aouf, L., Collard, F., 2010. Semi-empirical dissipation source functions for wind-wave models. Part I. Definition, calibration and validation. Journal of Physical Oceanography 40, 1917–1941.

Ardhuin, F., Tournadre, J., Queffeulou, P., Girard-Ardhuin, F., Collard, F., 2011a. Observation and parameterization of small icebergs: drifting breakwaters in the southern ocean. Ocean Modelling 39, 405–410.

Ardhuin, F., Stutzmann, E., Schimmel, M., Mangeney, D.A., 2011b. Ocean wave sources of seismic noise. Journal of Geophysical Research 116 (C9), C09004. http://dx.doi.org/10.1029/2011JC006952.

Atkinson, M., Smith, S.V., Stroup, E.D., 1981. Circulation in Enewetak atoll lagoon. Limnology Oceanography 26, 1074–1083.

Barruol, G., Reymond, D., Fontaine, F.R., Hyvernaud, O., Maurer, V., Maamaatuaiahutapu, K., 2006. Characterizing swells in the southern Pacific from seismic and infrasonic noise analyses. Geophysical Journal International 164, 516–542.

Benoit, M., Marcos, F., Becq, F. 1996. Development of a third generation shallow-water wave model with unstructured spatial meshing. In Proceedings of the 25th International Conference on Coastal Engineering, Orlando, ASCE, 465–478.

Burrows, M.T., Harvey, R., Robb, L., 2008. Wave exposure indices from digital coastlines and the prediction of rocky shore community structure. Marine Ecology-Progress Series 353, 1–12.

Callaghan, D.P., Nielsen, P., Gourlay, M.R., Ballock, T.E., 2006. Atoll lagoon flushing forced by waves. Coastal Engineering 53, 691–704.

Chawla, A., Tolman, H.L., 2008. Obstruction grids for spectral wave models. Ocean Modelling 22, 12–25.

Collard, F., Ardhuin, F., Chapron, B., 2009. Monitoring and analysis of ocean swell fields from space. New methods for routine observations. Journal of Geophysical Research-Oceans 114, C07023.

Dee, D.P., Uppala, S., 2009. Variational bias correction of satellite radiance data in ERA-interim reanalysis. Quarterly Journal of the Royal Meteorological Society 135, 1830–1841.

Delpey, M.T., Ardhuin, F., Collard, F., Chapron, B., 2010. Space-time structure of long ocean swell fields. Journal of Geophysical Research-Oceans 115, C12037.

Dumas, F., Le Gendre, R., Thomas, Y., Andréfouët, S., 2012. Tidal flushing and wind driven circulation of Ahe atoll lagoon (Tuamotu Archipelago, French Polynesia) from in situ observations and numerical modelling. Marine Pollution Bulletin 65, 425–440.

Edmunds, P.J., Leichter, J.J., Adjeroud, M., 2010. Landscape-scale variation in coral recruitment in Moorea, French Polynesia. Marine Ecology-Progress Series 414, 75–89.

Ekebom, J., Laihonen, P., Suominen, T., 2003. A GIS-based step-wise procedure for assessing physical exposure in fragmented archipelagos. Estuarine Coastal and Shelf Science 57, 887–898.

Goldberg, N.A., Kendrick, G.A., 2004. Effects of island groups, depth, and exposure to ocean waves on subtidal macroalgal assemblages in the Recherche archipelago, Western Australia. Journal of Phycology 40, 631–641.

Harborne, A., Mumby, P., Zychaluk, K., Hedley, J., Blackwell, P., 2006. Modeling the beta diversity of coral reefs. Ecology 87, 2871–2881.

Hoeke, R., Storlazzi, C., Ridd, P., 2011. Hydrodynamics of a bathymetrically complex fringing coral reef embayment: wave climate, in situ observations, and wave prediction. Journal of Geophysical Research-Oceans 116, C04018.

Hopley, D., 2011. Encyclopedia of Modern Coral Reefs. Structure, Form and Process. Springer, Berlin, pp. 1206.

Kraines, S., Susuki, A., Yanagi, T., Isobe, M., Guo, X., Komiyama, H., 1999. Rapid water exchange between the lagoon and the open ocean at Majuro Atoll due to wind, waves, and tide. Journal Geophysical Research 104, 15635–15654.

Kench, P.S., 1998. Physical processes in an Indian Ocean atoll. Coral Reefs 17, 155–168.

Madin, J.S., Connolly, S.R., 2006. Ecological consequences of major hydrodynamic disturbances on coral reefs. Nature 444, 477–480.

Magne, R., Ardhuin, F., Roland, A., 2010. Prévisions et rejeux des états de mer du globe à la plage (waves forecast and hindcast from global ocean to the beach). European Journal of Environmental and Civil Engineering 14, 149–162.

Pawka, S.S., Inman, D.L., Guza, R.T., 1984. Island sheltering of surface gravity-waves – model and experiment. Continental Shelf Research 3, 35–53.

Queffeulou, P., 2004. Long term validation of wave height measurements from altimeters. Marine Geodesy 27, 495–510.

Queffeulou, P., Croizé-Fillon, D., 2010. Global altimeter SWH data set, version 7, <ftp://ftp.ifremer.fr/ifremer/cersat/products/swath/altimeters/waves/>.

Queffeulou, P., 2011. Updated altimeter SWH validation for ENVISAT, Jason-1 and Jason-2. Technical Report, IFREMER, LOS, BP 70, 20280 Plouzané, France.

Saha, S. et al., 2010. The NCEP climate forecast system reanalysis. Bulletin of the American Meteorological Society 91, 1015–1057.

Soto, I., Andréfouët, S., Hu, C., Muller-Karger, F.E., Wall, C.C., Sheng, J., Hatcher, B.G., 2009. Physical connectivity in the Mesoamerican Barrier Reef System inferred from 9 years of ocean color observations. Coral Reefs 28, 415–425.

Storlazzi, C.D., Brown, E.K., Field, M.E., Rodgers, K., Jokiel, P.L., 2005. A model for wave control on coral breakage and species distribution in the Hawaiian Islands. Coral Reefs 24, 43–55.

Tartinville, B., Deleersnijder, E., Rancher, J., 1997. The water residence time in the Mururoa atoll lagoon: sensitivity analysis of a three-dimensional model. Coral Reefs 16, 193–203.

Tartinville, B., Rancher, J., 2000. Wave-induced flow over Mururoa atoll reef. Journal of Coastal Research 16, 776–781.

Thomas, Y., Le Gendre, R., Garen, P., Dumas, F., Andréfouët, S., 2012. Bivalve larvae transport and connectivity within the Ahe atoll lagoon (Tuamotu Archipelago), with application to pearl oyster aquaculture management. Marine Pollution Bulletin. 65, 441–452.

Tolman, H.L., 2003. Treatment of unresolved islands and ice in wind wave models. Ocean Modelling 5, 219–231.

Tolman, H.L., 2007. Automated grid generation for WAVEWATCH III. Technical Report 254, Environ. Canada, Toronto, Ont., Canada.

Tolman, H.L., 2008. A mosaic approach to wind wave modeling. Ocean Modelling 25, 35–47.

Tolman, H.L., 2009. User manual and system documentation of WAVEWATCH III™ version 3.14, Technical Report 276, NOAA/NWS/NCEP/MMAB.

Walker, S.J., Degnan, B.M., Hooper, J.N.A., Skilleter, G.A., 2008. Will increased storm disturbance affect the biodiversity of intertidal, nonscleractinian sessile fauna on coral reefs? Global Change Biology 14, 2755–2770.

Zieger, S., Vinoth, J., Young, I.R., 2009. Joint calibration of multiplatform altimeter measurements of wind speed and wave height over the past 20 years. Journal of Atmospheric and Oceanic Technology 26, 2549–2564.